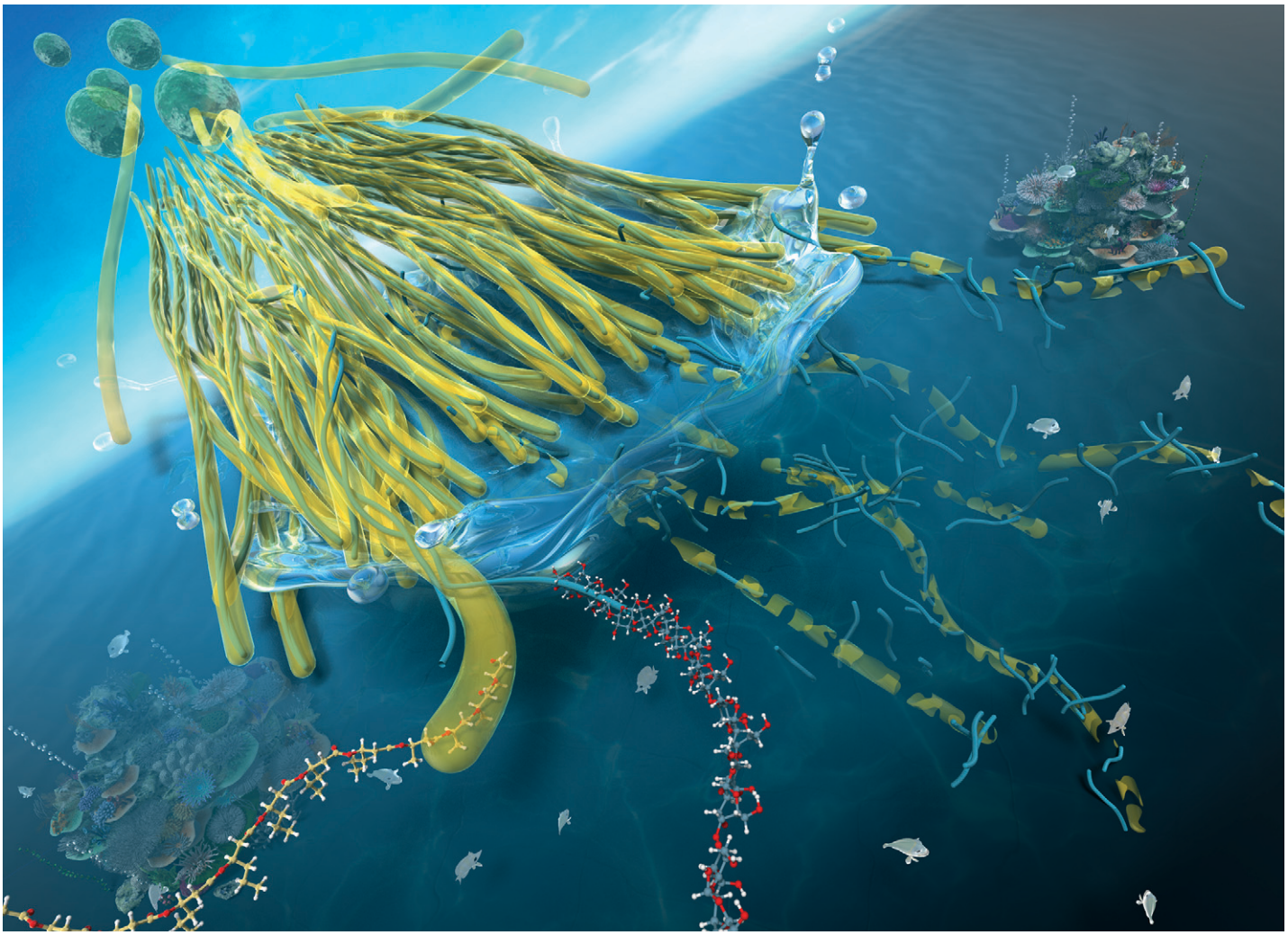

Featuring work from Prof. Satoshi Fujita at Department of Frontier Fiber Technology and Science, University of Fukui, Japan.

Seawater-degradable, tough, and fully bio-derived nonwoven polyester fibres reinforced with mechanically defibrated cellulose nanofibres

Electrospinning via Pickering emulsion yielded cellulose nanofiber-containing biopolyester nanofibrous nonwoven fabric, which exhibited excellent toughness. This entirely biomass-derived, seawater-degradable bioplastic fabric would be a “green” alternative to conventional polyester fabrics.

As featured in:

See Satoshi Fujita *et al.*, *Environ. Sci.: Nano*, 2023, **10**, 92.

ROYAL SOCIETY OF CHEMISTRY

rsc.li/es-nano

Registered charity number: 207890

Environmental Science Nano

ROYAL SOCIETY OF CHEMISTRY

PAPER

View Article Online
View Journal | View Issue

Cite this: *Environ. Sci.: Nano*, 2023, 10, 92

Seawater-degradable, tough, and fully bio-derived nonwoven polyester fibres reinforced with mechanically defibrated cellulose nanofibres†

Miyu Yamagata,[a] Yoshiyasu Nagakawa,[b] Mizuki Irie,[c] Shin-ichiro Suye[acd] and Satoshi Fujita *[acd]

Received 7th May 2022,
Accepted 10th October 2022

DOI: 10.1039/d2en00441k

rsc.li/es-nano

Developing nonwoven fabrics using sustainable materials is necessary to alleviate marine plastic pollution. Poly(3-hydroxybutyrate-co-3-hydroxyhexanoate) (PHBH) has attracted attention because it undergoes natural degradation, particularly in the ocean. Electrospun PHBH nonwoven fabrics have limited applications owing to poor mechanical properties. Although the use of cellulose nanofibres (CNFs) as fillers can potentially result in enhancement of the mechanical properties of PHBH nonwoven fabrics, their low dispersibility in $CHCl_3$, a good solvent for PHBH, hinders the direct electrospinning of CNF-containing PHBH. Herein, nonwoven fibres were fabricated directly by electrospinning Pickering emulsions stabilized with mechanically defibrated CNFs. The CNFs were found to be encapsulated in the core of the PHBH fibres. CNF-reinforced fibres showed excellent toughness, approximately 11 and 22 times greater than those of PHBH films and CNF-free PHBH fibres, respectively. These also underwent complete and very rapid degradation in seawater (7–10 d), compared to the PHBH film (14–40 d). The proposed CNF-reinforced PHBH is a seawater-degradable bioplastic containing complete biomass-derived components.

Environmental significance

Nonwoven fabrics widely used in various industries are mainly made of synthetic polymers, which cause marine pollution by breaking down to microplastics. Seawater-degradable nonwoven fabrics are highly desired but have not yet been put to practical use. Herein, PHBH, which has seawater-degradability but low toughness, was used in the manufacture of nonwoven nanofibrous fabrics by blending with CNFs. Electrospinning *via* Pickering emulsion yielded CNF-containing PHBH fibres, which exhibited excellent toughness despite using only a small amount of CNF. This entirely biomass-derived, seawater-degradable bioplastic nonwoven fabric would be a "green" alternative to conventional polyester nonwoven fabrics. This approach would also be a promising method to fabricate CNF-hybrid plastics.

1. Introduction

In response to COVID-19, nonwoven fabrics have emerged as an expanding field in textile products for various applications including clothing, medical devices, hygiene products, and other industries.[1] Most nonwoven products are made of petrochemical-based thermoplastics, such as polyethylene terephthalate, polypropylene, and polyethylene, which are non-biodegradable.[2] Such disposable nonwoven products with a relatively short service life can cause serious environmental issues. For example, discarded surgical masks with a release rate of 396 billion microplastics per day contribute to marine microplastic pollution.[1] The global inclination toward sustainability has driven a strong interest in the use of biodegradable renewable bio-based materials for nonwoven fabrics.[1–3] Polyhydroxyalkanoates, which are polyesters produced by microorganisms, have attracted attention as a potential solution to these issues. In particular, poly(3-hydroxybutyrate-*co*-3-hydroxyhexanoate) (PHBH) is expected to mitigate marine microplastic pollution efficiently because it is completely converted into CO_2 and water upon enzymatic degradation by microorganisms in the ocean.[4–7] PHBH has been extensively used to fabricate plastic bags and disposable straws,[8] and has been investigated for fiberization into micrometre-sized fibres using melt-spun blowing.[9,10] Electrospinning, an efficient method for obtaining nonwoven fabrics with nanometre-sized fibres, can also be applied to

[a] *Department of Frontier Fiber Technology and Sciences, Graduate School of Engineering, University of Fukui, 3-9-1, Bunkyo, Fukui 910-8507, Japan*
[b] *Biotechnology Group, Tokyo Metropolitan Industrial Technology Research Institute, 2-4-10, Aomi, Koto-ku, Tokyo 135-0064, Japan*
[c] *Department of Materials Science and Biotechnology, Faculty of Engineering, University of Fukui, 3-9-1, Bunkyo, Fukui 910-8507, Japan*
[d] *Organization for Life Science Advancement Programs, University of Fukui, 3-9-1, Bunkyo, Fukui 910-8507, Japan*

† Electronic supplementary information (ESI) available. See DOI: https://doi.org/10.1039/d2en00441k

PHBH, but electrospun nonwoven PHBH fibres exhibit poor mechanical properties.[11–13] Fillers such as nanosilica,[14] montmorillonite,[15] carbon nanotubes,[16] and glass fibres[17] have been used to enhance the mechanical characteristics of PHBH. However, challenges remain in the use of fillers for sustainable biodegradable polymers.

Cellulose nanofibres (CNFs) are prepared by finely disassembling plant fibres, such as pulp and wood chips, into nanosized fibres. As these are bio-based biodegradable materials, CNFs are attracting attention as a next-generation renewable organic resource that can facilitate the transition toward a sustainable society with minimal environmental impact.[18] CNFs have also received considerable attention as alternative fillers to carbon and glass fibres because of their high strength, lightweight, and low cost.[19–21] CNFs do not cause any environmental problems even if they are released into the ocean, which demonstrates their potential to be used as an ideal filler for seawater-degradable plastics. Our group has found that electrospun nanofibres can be strengthened *via* the addition of CNFs.[22] CNF-reinforced composite PHBH nonwoven fabrics are expected to be extensively applied as novel, completely bio-based, and seawater-degradable materials. However, as CNFs are hydrophilic and polymers including PHBH are usually hydrophobic, the low dispersibility of CNFs in polymers poses a challenge in their use as a filler. CNF surfaces have been chemically treated to disperse CNFs as fillers in polymers. The dispersibility of CNFs can be improved by introducing hydrophobic functional groups, such as 3-isocyanatopropyl triethoxysilane[23] and benzoic acid anhydride,[24] and ionic functional groups, such as tannic acid[25] and epoxypropyltrimethylammonium chloride.[26] However, a simple chemical-treatment-free method for blending CNFs with polymers is still desired to avoid the routinely adopted chemical treatments of CNFs in these investigations. Here, Pickering emulsions containing CNFs were used to achieve a thorough blend of CNF with PHBH. Pickering emulsions, which are stabilized by the adsorption of solid particles on the interface between the two phases in the emulsion,[27] were targeted in the present study. Owing to their amphiphilicity, mechanically defibrated CNFs can stabilize oil-in-water (o/w) emulsions by forming a network-like fibre structure on the interface.[28,29] It has previously been demonstrated that simple casting of Pickering emulsions does not result in sufficient mechanical strength because of the agglomeration of CNFs.[30–32] To the best of our knowledge, electrospinning of PHBH incorporated CNF has never been reported. This study focused on the electrospinning of Pickering emulsion to prepare CNF-incorporated fibres.

It is expected that the direct electrospinning of Pickering emulsions containing hydrophobic polymers and mechanically defibrated untreated CNFs can yield CNF-containing nonwoven fabrics *via* a simple manufacturing process. In this study, CNF-reinforced PHBH-nanofibre-based nonwoven fibres were fabricated using Pickering emulsions, and their superior mechanical properties and seawater degradability were demonstrated. These results highlight the potential of PHBH as a sustainable nonwoven material.

2. Experimental

2.1. Preparation of samples

PHBH powder (containing 10.6 mol% poly-3-hydroxyhexanoate; Kaneka, Osaka, Japan) was dissolved in $CHCl_3$ (Fujifilm Wako, Osaka, Japan) and stirred overnight to prepare a 20% PHBH solution. To investigate the effects of the length and concentration of CNFs on the mechanical properties, long and short CNFs (Ima-10005 and Fma-10005, respectively; BiNFi-s; Sugino Machine, Toyama, Japan) were suspended in water, vortexed, and sonicated (40 kHz, 110 W, 10 min) to prepare 1.0%, 2.0%, 3.0%, and 4.0% CNF suspensions. The PHBH/$CHCl_3$ solution and CNF/water suspensions were mixed at a volume ratio of 3 : 1. Three cycles of vortexing (30 s) and sonication (5 min) were executed to prepare the Pickering emulsions. Table S1† presents the compositions of the prepared emulsions and fabricated fibres. The S- and L-prefixes in the sample notations indicate short and long CNFs, respectively, and the numbers represent the final composition of the CNFs in the synthesized materials. For example, the L-6.3 fibres contain 6.3% long CNFs dispersed in the PHBH matrix.

Fibres were obtained by electrospinning (NANON; MECC, Fukuoka, Japan), which involves spraying of a polymer solution through application of a high voltage to a grounded collector.[11,12] Electrospinning was performed by injecting the emulsions through a 22G spinneret at a flow rate of 0.4 mL h^{-1} and an electric field of 1.25 kV cm^{-1}, which yielded fibre sheets on a drum collector rotating at a linear velocity of 3.1 or 12.6 m s^{-1}. For comparison, cast films were prepared by spreading the emulsion over a φ 100 mm glass dish and drying overnight at 25 °C.

2.2. Characterization of fabricated materials

Scanning electron microscopy (SEM). Surface morphologies were analysed using SEM (JSM-6390FMM, JEOL, Tokyo, Japan) at an applied voltage of 15 kV. The SEM samples were coated with Pt/Pd (120 s, 15 mA, 6 Pa) using an ion coater. The fibre diameter and orientation, which affect the mechanical properties of the fibre sheets, were determined from the SEM images using ImageJ software (ver. 1.52e). To measure the orientation of the fibres, power spectra were obtained from the original images by Fourier transformation.[22] The intensity was discreetly integrated as a function of the angle from the frequency origin. The second-order parameter, S, was calculated from the aforementioned distribution, as shown in eqn (1), where θ is the orientation angle and the angle brackets represent the averaged value.

$$S = 2\langle\cos^2\theta\rangle - 1 = \langle\cos 2\theta\rangle \quad (1)$$

Transmission electron microscopy (TEM). The internal structures of single fibres were examined by TEM (H-7650,

Hitachi, Tokyo, Japan) at voltages of 100–200 kV. Samples were loaded on a carbon support membrane (ELS-C10; φ 3 mm; Okenshoji, Tokyo, Japan) that was hydrophilized by oxygen plasma treatment (75 s, 5 mA; PIB-10, Vacuum Devices, Ibaraki, Japan). A CNF suspension (0.01%) was dropped onto the membrane and dried. The fibres were directly electrospun on the membrane for 10 s.

Tensile tests. To evaluate the mechanical properties of the fibre sheets, 10 × 15 mm specimens were analysed using a KES-G1SH tensile tester (Kato Tech, Kyoto, Japan) under the following conditions: load cell, 1 kg; gap between grips, 50 mm; and tensile speed, 0.05 mm s^{-1}. For each sample, the measurements were performed three times in the axial direction of the fibres. The thicknesses of the specimens were measured using a micrometre. The elastic moduli were calculated from the initial slope of the obtained curves, and the tensile strength and uniform elongation were determined from the data collected at maximum stress. Toughness was calculated using the area under the stress–strain curve.

Water contact angle (WCA) measurements. Surface hydrophilicity was examined by WCA analysis. A water droplet (5 μL) was placed on a specimen that was electrospun onto a glass slip, and the WCA was measured after 2 s of dropping using a drop shape analyser (DSA-20, Krüss, Hamburg, Germany) with the tangential method. The measurements were repeated five times for each sample.

Attenuated total reflectance-Fourier transform infrared (ATR-FTIR) spectrometry. ATR-FTIR measurements were performed to determine the functional groups of the fibres. A Nicolet 6700 system (Thermo Scientific, Waltham, MA, USA) was used to collect ATR-FTIR spectra in the 400–4000 cm^{-1} range; an average of 64 scans was acquired at a resolution of 4 cm^{-1} and an angle of incidence of 45°.

Small-angle X-ray scattering (SAXS). SAXS measurements were acquired using a SAXSpoint5.0 instrument (Anton Paar, Graz, Austria) at a wavelength (λ) of 0.1542 nm. Two-dimensional (2D) scattering data were collected using an X-ray Eiger2 R 1M detector (Dectris, Zürich, Switzerland). The specimens were set parallel and perpendicular to the meridional axis of the X-ray detector to analyse structures that were parallel and perpendicular to the fibre axes. The scattering vector, $q = (4\pi/\lambda)\sin\theta$, where θ is the scattering angle, was calibrated using silver behenate. One-dimensional (1D) profiles were acquired by sector-averaging the 2D SAXS patterns within a sector angle of 45° with the meridional axis. Structures with a long period ($2\pi/q$) were evaluated according to Bragg's law, where q is the value of the peak (q_{max}) in the $q^2I(q) - q$ plot.[33]

Gel permeation chromatography (GPC). The molecular weight of PHBH was determined by GPC. A Shodex RI detector and column (Shodex, LF-804, 8.0 × 300 mm, i.d.) were employed at 40 °C with a flow rate of 0.6 mL min^{-1} for 30 min using $CHCl_3$ (HPLC grade, filtered) as the eluent. The samples were dissolved in HPLC-grade $CHCl_3$ at a concentration of 0.05 w/v%, and the solution was filtered (Millipore, SLLGH04NL, 0.2 μm) prior to GPC analysis. Polystyrene standards (Shodex) with low polydispersity were used to construct the calibration curve.

2.3. Evaluation of degradability

Degradability test. For *in situ* degradation tests, specimens measuring 2.5 × 2.5 cm^2 were cut and placed individually in 50 mL centrifuge tubes having six and three drilled holes (ø 3 mm) in the tube and cap, respectively, to enable seawater circulation. The tubes were immersed in a pump room and water tank at the Echizen Matsushima Aquarium. To avoid the effect of mechanical damage by waves or sand, *in vitro* degradation tests were also performed. Similar sized specimens (2.5 × 2.5 cm^2) were individually placed in tubes containing 40 mL of seawater. These tubes, with their caps loosened, were incubated at 25 °C, and the seawater was changed every 3–4 d. In both tests, to estimate the sample degradability, weight loss was measured. Periodically collected specimens were rinsed three times with water, freeze-dried, and stored in a freezer (−80 °C) for subsequent morphological and chemical analyses. Three specimens were tested for each examined duration. The weight loss of each specimen was obtained using eqn (2), where m_i is the initial weight and m_f is the weight after immersion.

$$\text{Weight Loss\%} = \frac{m_i - m_f}{m_i} \times 100 \quad (2)$$

Crystal violet staining. The samples subjected to *in vitro* degradation were stained with crystal violet, which stains peptidoglycans and sugars present in biofilms purple. Pieces of the samples were placed in a dish containing 10 mL of 0.1% crystal violet solution (Nacalai Tesque, Kyoto, Japan) for 20 min and subsequently washed three times with water for 3 min.

3. Results and discussion

3.1. Fabrication of CNF-incorporated PHBH fibres

The PHBH/$CHCl_3$ solutions and CNF/water suspensions were homogenized at a volume ratio of 3 : 1 to prepare Pickering emulsions. CNF-containing nonwoven fibres were obtained by electrospinning each emulsion onto a rotating collector (Fig. 1a). Mechanically defibrated CNFs with two different lengths were used. The shorter CNFs with an average length (estimated from microscopic observation of dispersion) of 722 ± 370 nm (Fig. S1b†) stood straight (Fig. 1b), whereas the longer CNFs, with an average length of 54 ± 26 μm (Fig. S1a†), were sufficiently long and flexible to entangle with each other (Fig. 1c). The small peak in the L-6.3 emulsion (Fig. S1a†) can be attributed to the presence of a small fragment of CNF in long CNF because a similar peak appears in a dilute suspension of long CNF. Well-stabilized emulsions were obtained for all the examined compositions (Table S1†). SEM analysis of the lyophilized cloudy L-6.3 emulsion revealed that the particle surfaces were covered with a fibrous structure (Fig. 1a). This observation suggests that the

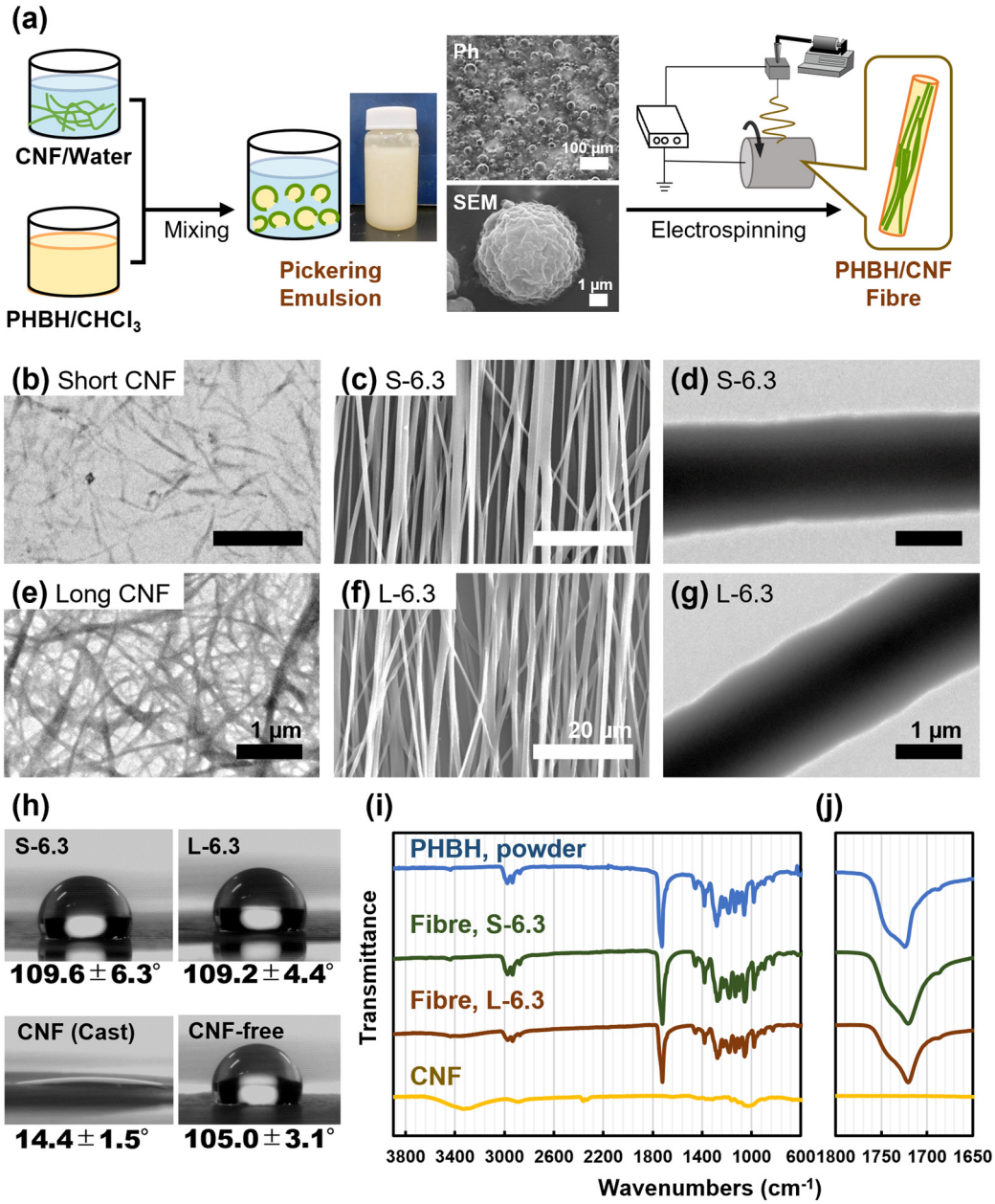

Fig. 1 (a) Preparation of CNF-containing PHBH fibres. A CNF/water suspension and PHBH/$CHCl_3$ solution are homogenized to form a Pickering emulsion, in which particles are enveloped by CNFs. Images of the L-6.3 emulsion are shown. Highly aligned CNF-containing PHBH fibres are obtained *via* direct electrospinning of the emulsion onto a rotating collector. (b–g) Morphological analysis. SEM images of (b and e) CNFs and (c and f) electrospun aligned sheets of CNF-containing fibres collected at a high speed (12.6 m s^{-1}). (d and g) TEM image of a single CNF-containing fibre. (b–d) and (e–g) show short and long CNFs, respectively. (h) WCAs of CNF cast film and the S-6.3, L-6.3, and CNF-free fibre sheets. (i) ATR-FTIR spectra of PHBH, S-6.3 fibres, L-6.3 fibres, and CNFs. (j) Enlarged region highlighting the C=O-derived peaks.

continuous layer of the emulsion was aqueous and that the particles were o/w emulsions consisting of a PHBH/$CHCl_3$ phase surrounded by CNFs. Dynamic light scattering (DLS) analysis indicated that the L-6.3 and S-6.3 emulsions had wide diameter distributions, with averages of approximately 1160 and 3410 nm, respectively (Fig. S2†). Mechanically defibrated CNFs are amphiphilic and their hydrophilicity is governed by the degree of mechanical fibrillation.[34] Since the formation of Pickering emulsion is affected by the hydrophilicity of CNF, the emulsion size would be affected by the CNF length because it contributed to the different hydrophilicity of CNF.

Fibre sheets were prepared by electrospinning the emulsions. Highly oriented fibres with a smooth surface and no beading were obtained by rotating the collector at a high speed (12.6 m s^{-1}) (Fig. 1c and f). Regardless of the length and concentration of the added CNFs, the average diameter obtained was ~1.2 μm and the second-order parameter, *S*,

was always greater than 0.8, indicating that the electrospun fibres were well-oriented (Fig. S3†). Thinner fibres were obtained by stretching during electrospinning onto the high-speed rotating collector. Electrospinning performed by rotating the collector at a low speed (3.1 m s^{-1}) yielded randomly oriented fibres (S = 0.257) with smooth surfaces and minimal beading (Fig. S4†). The average diameter of these randomly oriented fibres (~1.7 μm) was greater than that of the oriented fibres. The sizes of the emulsions and the diameters of the prepared fibres did not appear to be directly related, which was expected because the emulsions collapsed in the Taylor cones during electrospinning.

3.2. Characterization of electrospun fibres

Electron microscopy. TEM was used to reveal a region of high electron density in the core regions of the short- and long-CNF-containing fibres (Fig. 1d and g). The analysis suggested that the CNFs were present in the fibre interior, especially in the core regions, in a continuously agglomerated manner, as found in a previous study.[22] The contrast between the core and shell was unclear, which indicates that the core phase was not only composed of CNF but also of PHBH, and that the interface was interpenetrating. The inversion in the localisation that can be predicted from the structure of Pickering emulsion can be explained as a phenomenon in which functional groups with low surface free energies are exposed on the surface of fibres electrospun in the gas phase.[35] The emulsion surrounded by CNFs presumably collapses at the Taylor cone during injection, enclosing the hydrophilic CNFs and exposing the hydrophobic PHBH/$CHCl_3$ phase with a low surface free energy on the surface. Notably, certain fibres with darker asymmetric contrast on one side were observed (Fig. S5†), implying that the difference, in contrast, was not an artifact of the curvature of the fibre surface.

To directly observe the internal structure of the fibres, these were frozen in liquid nitrogen and then sectioned. The cross sections were observed using SEM. A spike-like structure was observed in the core of L-6.3 fibres (Fig. S6a†), indicating that the L-6.3 fibres contained CNF in their cores, whereas the CNF-free fibres observed for comparison were smooth and homogeneous (Fig. S6b†).

WCA analysis. The surface properties of fibres significantly affect the penetration of water and adhesion of bacteria, leading to specific biodegradability. Surface WCA measurements were performed to investigate the surface properties of the electrospun fibres (Fig. 1h and S7†). The CNF film and CNF-free PHBH fibre sheet had hydrophilic (14.4° ± 1.5°) and hydrophobic (105.0° ± 3.1°) surfaces, respectively. With respect to the CNF-containing fibres, S-6.3 and L-6.3 showed WCAs of 109.6° ± 6.3° and 109.2° ± 4.4°, respectively, which were comparable to that of the PHBH sample. These results also suggested that the fibres electrospun from the Pickering emulsions have PHBH surfaces that encapsulate the CNFs.

ATR-FTIR. In ATR-FTIR analysis, the penetration depth of the infrared light is greater than the fibre diameter; however, the apparent penetration depth during measurements of electrospun fibre sheets is considerably smaller than the fibre diameter because of the large interfibre voids present in porous fibre sheets.[36,37] Therefore, information related to the surface of a single fibre is important. If the CNF region was localised on the outside of the fibres, a CNF-derived peak would be observed. However, no CNF-derived peaks were clearly identified (Fig. 1i), possibly because of the low content of CNFs and their encapsulation within the fibres. The characteristic peak of PHBH at 1719 cm^{-1} (C═O str.)[38] red-shifted upon the addition of CNFs (Fig. 1j), suggesting that C═O could be involved in the hydrogen bonding between PHBH and the CNFs.

SAXS analysis. To analyse the aggregation of CNFs in the fibres, aligned L-6.3 fibres, aligned CNF-free fibres, a L-6.3 film, and a CNF-free film were also analysed by SAXS. The 2D plots of the fibre sheet, acquired perpendicular and parallel to the fibre axis were integrated with the meridian direction at an aperture angle of 45° and plotted in one dimension (Fig. 2). Strong streaks perpendicular to the fibre axis were observed in the CNF-free fibres, whereas less intense streaks were observed in the CNF-containing fibres (Fig. 2f). The intensity of the CNF-containing fibres was proportional to q^{-4} with q ranging from 0.05 to 0.5 nm^{-1}, for both parallel and perpendicular directions to the fibre axis (Fig. 2g). These results followed Porod's law,[39,40] suggesting that each fibril of the CNFs was not aligned with the fibre but aggregated in it. These results indicate the presence of a continuous core containing densely entangled CNFs in the fibres, which is also supported by the TEM findings. A peak was observed at q_{max} of approximately 1 nm^{-1} ($d \approx 6.3$ nm), which could be attributed to a long-period structure between the crystalline and amorphous regions of PHBH. The fibres showed higher q values than the films because an extension occurred during electrospinning; however, the presence of CNFs did not affect the position of q_{max}, that is, the size of the long-period structure. This result supports the hypothesis that CNFs and PHBH are primarily localised in the core and shell regions, respectively.

Mechanical properties. The mechanical strength of the CNF-containing fibre sheets was evaluated using tensile tests. The CNF-free fibres ruptured immediately after reaching the yield point, whereas the CNF-containing fibres were significantly elongated even after the yield point (Fig. 3a). The CNF-incorporated L-6.3 fibres showed significant increase in elastic modulus (22.3 ± 7.0 to 92.0 ± 9.5 MPa; 4.1 times) and tensile strength (2.3 ± 0.8 to 8.0 ± 2.0 MPa; 3.5 times); additionally, their toughness was drastically improved (0.2 ± 0.04 to 4.4 ± 0.4 MPa; 22 times) (Fig. 3b). In general, a CNF content of 10–30% is required in a filler to improve mechanical properties.[41,42] Interestingly, the method reported herein dramatically improved the tensile strength, uniform elongation, and toughness of the nonwoven fibres by 3.5, 4.4, and 22 times, respectively, with the addition of

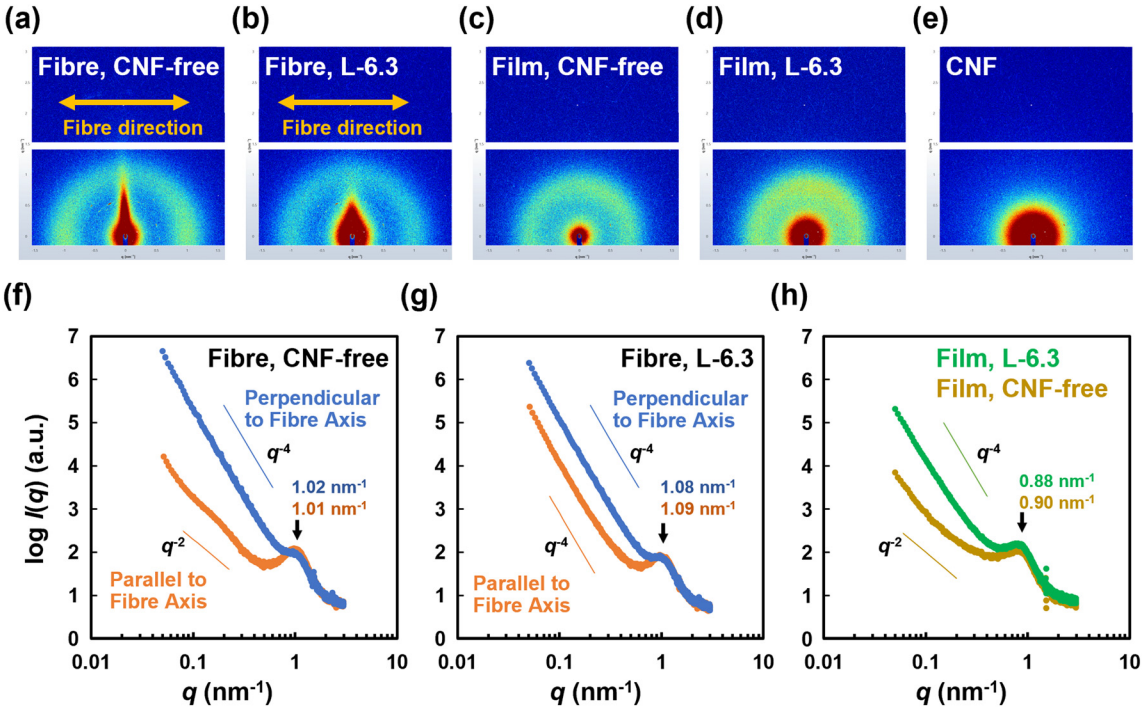

Fig. 2 (a–e) 2D SAXS profiles. (a) Aligned CNF-free fibres, (b) aligned L-6.3 fibres, (c) CNF-free film, (d) L-6.3 film, and (e) CNF cast film. Arrows indicate the direction of fibre alignment. (f–h) 1D SAXS profiles. (f) CNF-free PHBH fibres, (g) CNF-containing aligned fibres, and (h) films with and without CNFs.

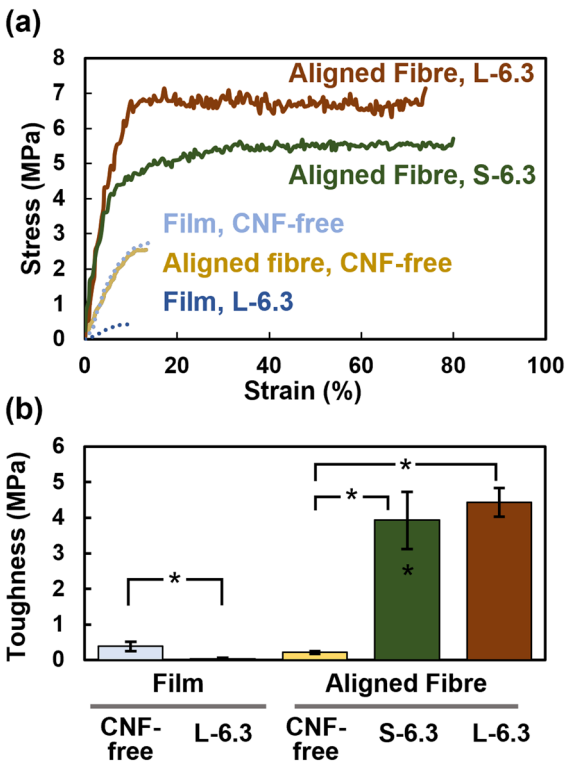

Fig. 3 (a) Stress–strain curves and (b) toughness data of aligned L-6.3 and S-6.3 fibres, CNF-free fibres, and L-6.3-based and CNF-free films (brown, green, yellow, blue, and cyan profiles, respectively). Asterisks represent a significant difference ($p < 0.05$).

only 6.3% CNF. The addition of a higher concentration of CNF is expected to further improve the mechanical strength; however, this was not investigated owing to the limitations of the concentration of CNF provided as a slurry.

The fabricated films were also analysed for comparison. The elastic modulus, tensile strength, and toughness of the pristine film decreased from 29.1 ± 13.1 to 5.8 ± 1.7 MPa, 3.5 ± 0.9 to 0.6 ± 0.4 MPa, and 0.4 ± 0.1 to 0.03 ± 0.02 MPa, respectively, upon the addition of CNFs. This behaviour could be due to the nonuniform aggregation of CNFs during film fabrication, which contributes to breakage in the thin PHBH region of the film. In contrast, the CNFs did not locally aggregate inside the electrospun fibres, which instead displayed a continuous core–shell-like structure that presumably enabled their high toughness. The effects of the CNF length and concentration as well as the orientation of the fibre sheet were also examined (Fig. S8 and S9†).

The stress–strain curves indicate that the stress remained constant, whereas the strain increased after the yield point, without any grip slippage or fibre breakage. These results were obtained presumably because of the presence of a high-density CNF core inside the fibres, entangled CNFs that hindered fibre breakage, and a CNF core that stretched as the fibre elongated. The intense interfacial interactions between the CNFs and PHBH might also have contributed to the toughness.

A SEM image of the fracture surface of S-6.3 fibre after tensile testing shows that no CNF protrusions were observed in the cross-section image of the fracture surface of S-6.3

fibre (Fig. S6c†). This indicates that the rupture during elongation may have occurred in the PHBH rather than the CNF section.

3.3. Evaluation of seawater degradability

***In situ* degradation tests.** The seawater degradability of the L-6.3 fibre sheet and film was analysed, with the CNF-free fibres and film used as controls. The *in situ* degradation test was performed in the pump room at the Echizen Matsushima Aquarium, in which fresh seawater containing mud, sand, and pieces of seaweed is constantly supplied directly from the sea, and the influence of tidal cycles is minimal (Fig. S10a†). The samples were immersed in seawater from September 28 to November 19, 2021; moreover, the seawater temperature was uncontrolled and identical to that of the sea (approximately 18–25 °C). The fibre sheets degraded faster than the films, beginning to collapse after 7 d and completely degrading within 1 month (Fig. 4a). In particular, L-6.3 completely degraded within 21 d, compared to 28 d for the CNF-free fibre sheet (Fig. 4b). In contrast, the films became cloudy over time and degraded by more than 34% within 42 d.

A similar experiment conducted in a water tank, which was not influenced by tides, mud, sand, and seaweed (Fig. S10b†), showed similar results but with increased degradation (Fig. S11†). This observation suggests that degradation was not induced by physical influences such as waves and sand but by microbes. Degradation was promoted in a fresh-seawater-based environment suitable for aerobic microorganisms, and differences in the microbial growth environments affected the degradation rates. The reason for the faster degradation of the fibre in comparison to the film would be the larger specific surface area of the fibre, which allowed more microorganisms to adhere.[43,44]

***In vitro* degradation tests.** *In vitro* degradation tests were conducted in a laboratory incubator in a controlled environment. Samples immersed in seawater collected from

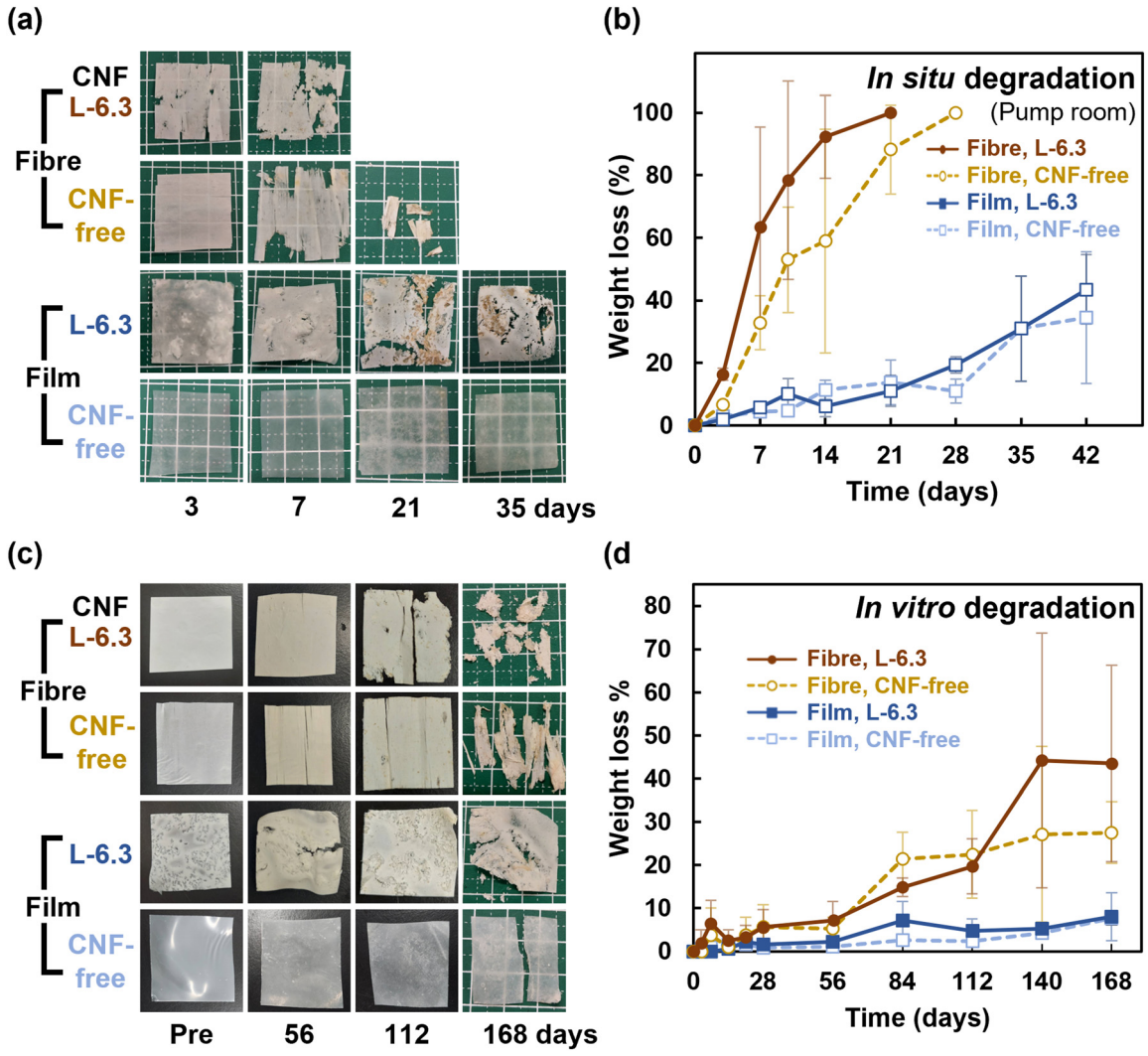

Fig. 4 Seawater degradation tests of fibre sheets and films with/without CNFs: (a and b) *in situ* (pump room) and (c and d) *in vitro* experiments. (a and c) and (b and d) show apparent morphology and weight loss data of the specimens, respectively.

a beach (Mikuni-cho, Fukui; 36°15′02″N, 136°08′17″E; sampled on July 1, August 5, September 28, and November 17, 2021) were incubated at 25 °C. Several pits were observed on the surfaces of both the CNF-containing and CNF-free fibre sheets after 84 d, and these samples disintegrated into several fragments after 140 d (Fig. 4c). In contrast, the film-based sheets became cloudy with increasingly roughened surfaces over time; moreover, their shapes were retained beyond 168 d. The fibres degraded more rapidly than the films because of their high specific surface areas. Certain areas of the CNF-containing film ruptured after 56 d (Fig. 4c). Quantitative results related to weight loss validated that the fibres degraded more rapidly than the films, especially after 112 d. Furthermore, the CNF-containing fibres degraded faster than the CNF-free fibres (Fig. 4d).

Morphological analysis. SEM analysis of the fibre samples that were immersed for 112 d *in vitro* and 7 d *in situ* revealed that several fibres became thinner and a few ruptured (Fig. 5). The surface roughness increased on not only the exterior of the sheets but also the interior, indicating that degradation occurred throughout the sheets. The films also showed an increase in surface roughness and a few holes. This tendency was observed for both long-term *in vitro* and short-term *in situ* immersions (Fig. 5). The L-6.3 fibres exhibited disrupted fibre orientation along with many cleaved fibres as degradation continued, whereas the orientation direction was preserved in CNF-free fibres. The TEM analysis of CNF-containing fibres (Fig. 1d and g) indicated that CNFs were bundled in the core of the fibres. As the degradation of the CNF-containing fibres progressed and reached the CNF core layer inside the fibre, the fibre was degraded from the core because the CNF is a good scaffold for microorganisms, causing faster degradation.[45]

Digestion of polymer chains. The molecular weights of the remaining samples in the *in vitro* test apparatus were determined by GPC (Fig. 6). The weight-average molecular weight (M_w) did not change; however, the number-average molecular weight (M_n) decreased, especially for the fibres. The degradation presumably proceeded in an exo-type manner because nonenzymatic hydrolysis would result in endo-type cleavage, in which the polymer chain is digested from the middle of the chain, leading to a decreased weight-average molecular weight. Certain microorganisms function *via* exo-type degradation with lipases to degrade a few types of polymers.[46,47] Similar enzymes could be produced during the bacterial degradation reported herein. No significant difference in the degradation behaviour was observed with or without the addition of CNFs, suggesting that the CNFs did not affect the degradation mechanism of PHBH.

Bacterial proliferation. To investigate bacterial proliferation, specimens were stained with crystal violet. Prior to the degradation tests, only the L-6.3 film showed a stained speckled pattern (Fig. 7). This was possibly because of the staining of CNFs that were aggregated and exposed on the film surface when it was cast. After immersion for 3 d, the film samples appeared similar to those prior to immersion

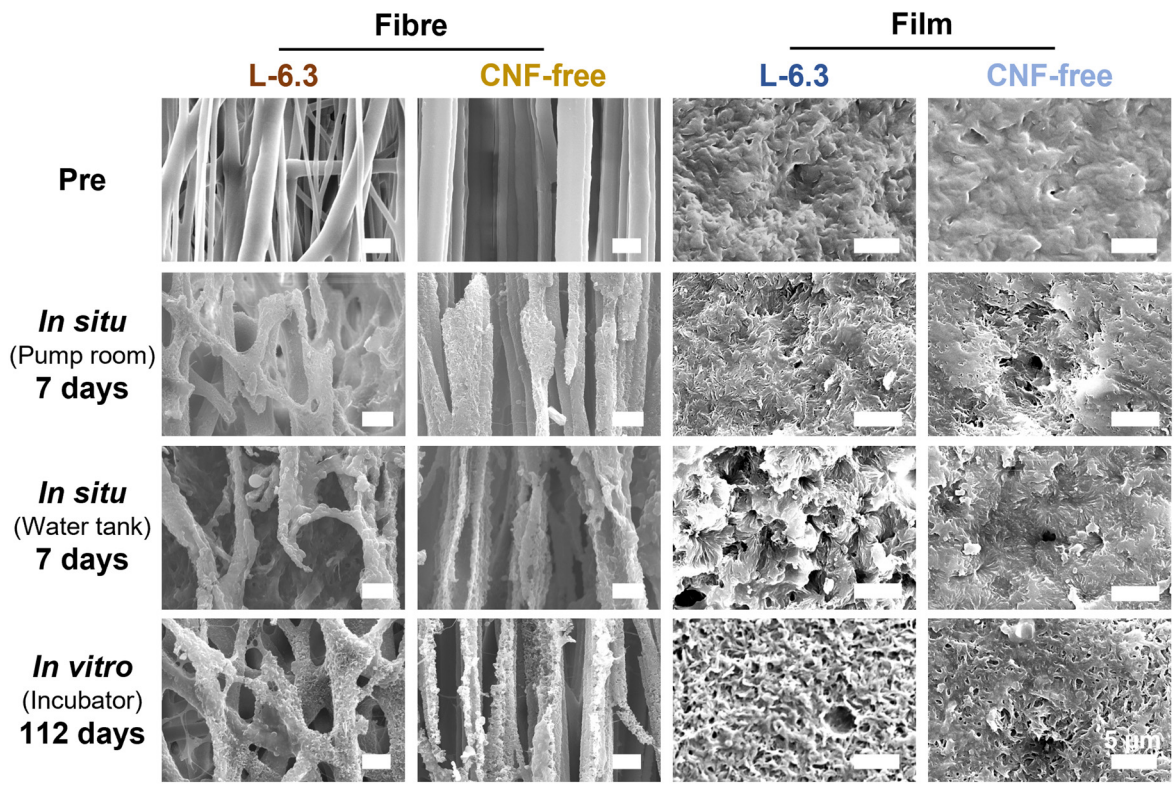

Fig. 5 SEM images of specimens before and after degradation tests (scale bar = 5 μm).

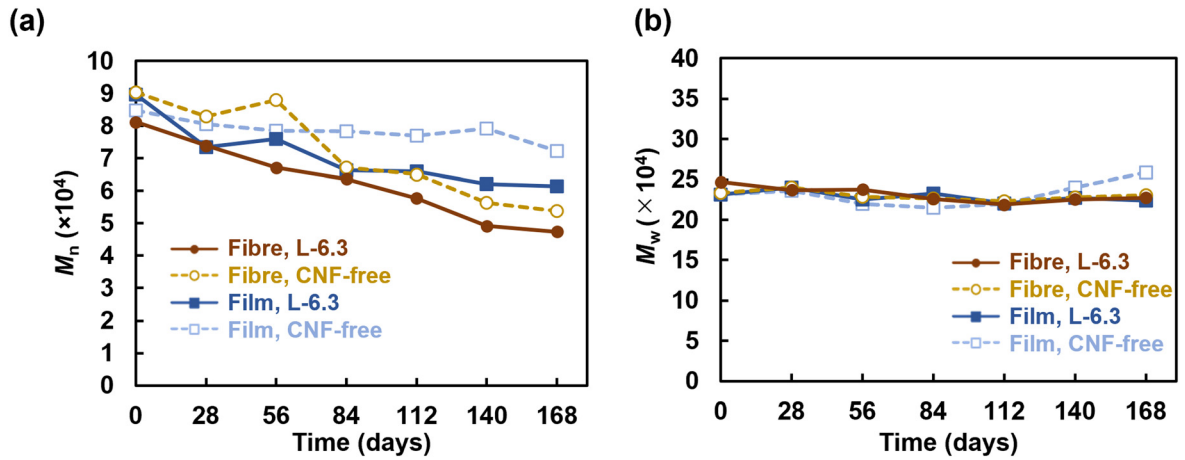

Fig. 6 GPC analysis results: (a) number-average molecular weight, M_n, (b) weight-average molecular weight, M_w, and (c) polydispersity index, M_w/M_n.

and showed no significant changes, suggesting that biofilm formation had not yet occurred. The fibre samples showed a small amount of biofilm formation after 3 d of immersion. All the samples were stained purple after 140 d of immersion, indicating biofilm formation. The staining was particularly intense in the fibre sheet, possibly because the larger surface area of the fibres enabled the adhesion of more microorganisms. Membrane-like structures with a biofilm-like appearance were observed in certain immersed samples; moreover, spherical bacteria and their aggregates were observed inside the membranes (Fig. 5 and S12†).

Regarding biodegradability, PHBH has been reported to be degraded by *Alteromonadaceae* in seawater.[48] Volant *et al.* reported that PHBH microbeads enclosed in a container with seawater and sand degraded by 80% in 250 d.[49] Sashiwa *et al.* found that PHBH powder degraded by 31% in 28 d.[5] The film fabricated in the present study degraded by 50% in 14–40 d in a natural environment, which is comparable to the degradation behaviour observed in previous studies.[5] In contrast, more than 50% of the fibre sheets degraded in 7–10 d and almost completely degraded within ~2 weeks. The high degradability of the fibres can be explained by the enhancement of hydrolysis owing to their larger specific surface area.[50] Microbial biofilms did not readily form on the surface of PHBH film because of its hydrophobicity (Fig. 7); however, the fibres provided a porous microenvironment suitable for bacterial adhesion and growth, resulting in high biodegradation. *In situ* degradation was remarkably faster than its *in vitro* equivalent. The influences of water currents and mud were considered. However, rapid degradation was also observed in the water tank without these influences, suggesting that microbial growth was promoted in the environment where seawater was constantly supplied. The *in vitro* degradation tests showed that neither the fibre sheets nor the films degraded significantly after approximately 1 month of immersion; however, rapid degradation was realized after 3 months of immersion. This observation is consistent with the exponential increase in the microorganism content. The degradation of the CNF-containing fibres was accelerated, particularly during the later period. This behaviour could be due to the encapsulation of the CNFs in the fibres during the early degradation stage. However, certain CNFs disintegrated as degradation progressed, and the microorganisms could readily penetrate the voids created by the loss of these CNFs, thereby accelerating degradation in both the exterior and interior parts of the fibres in the later period. The formation of microbial flora on the fibre sheets would enable the sheets to be used as a platform for the culture of polymer-degrading bacteria, thus facilitating investigations into the bacteria and enzymes involved in degradation.

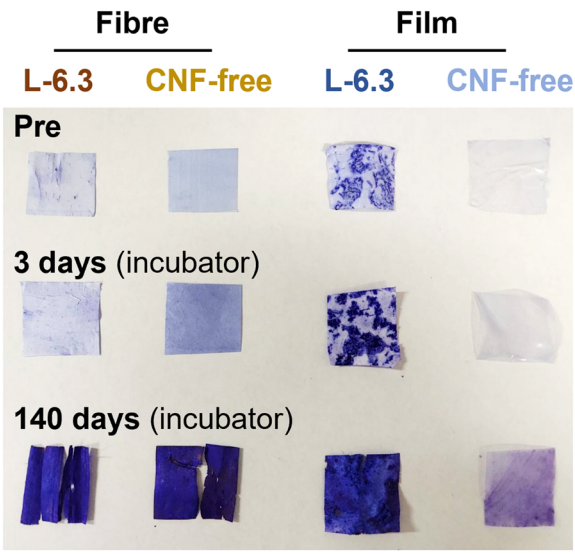

Fig. 7 (a) Crystal violet staining of specimens before and after degradation tests. SEM images of degraded aligned L-6.3 fibres after (b) *in situ* immersion (pump room) for 7 d, (c) *in situ* immersion (water tank) for 7 d, and (d) *in vitro* immersion for 112 d.

4. Conclusions

CNF-containing PHBH nonwoven fibres exhibited a higher elastic modulus, tensile strength, and uniform elongation than the PHBH fibres and CNF-free film. In particular, the oriented L-6.3 fibres showed high toughness, which was 11-times and 22-times greater than that of the PHBH films and CNF-free fibres, respectively. These properties can be attributed to the densely entangled CNF core within the fibres and the hydrogen bonds at the CNF–PHBH interface. The CNF-containing fibres were degraded by microorganisms in seawater within 7–10 d, which was much more rapid than the degradation of the PHBH films and CNF-free fibres. The chemical treatment of CNF surfaces is a common approach for dispersing CNFs in hydrophobic polymer matrices; however, the electrospinning of Pickering emulsions is a simpler method for mass production because mechanically defibrated CNFs can be directly used. Moreover, the CNF-reinforced nonwoven PHBH fibres are a fully bio-derived plastic, that is, born from and returned to nature, because both the CNFs and PHBH are derived from biomass and are biodegradable. This material can potentially contribute to breaking away from a petroleum-based society and solving marine plastic pollution.

Author contributions

Miyu Yamagata: data curation, methodology, writing–original draft, and visualization. Yoshiyasu Nagakawa: data curation, methodology, and investigation. Shin-ichiro Suye: writing–reviewing and editing. Satoshi Fujita: conceptualization, methodology, investigation, validation, writing–original draft, reviewing, and editing.

Conflicts of interest

There are no conflicts to declare.

Acknowledgements

This study was supported by a JSPS KAKENHI grant (No. 21K04686) and research grants from University of Fukui (FY 2021). The authors are grateful to Dr. Shunsuke Sato for fruitful discussions; Mr. Takashi Suzuki and Dr. Seiji Sasai (Echizen Matsushima Aquarium) for their cooperation with the degradation tests; and Editage (**https://www.editage.jp**) for English proofing.

References

1 J. Sun, S. Yang, G.-J. Zhou, K. Zhang, Y. Lu, Q. Jin, P. K. S. Lam, K. M. Y. Leung and Y. He, *Environ. Sci. Technol. Lett.*, 2021, **8**, 1065–1070.
2 G. Bhat and D. V. Parikh, in *Applications of Nonwovens in Technical Textiles*, Elsevier, 2010, pp. 46–62.
3 A. S. Santos, P. J. T. Ferreira and T. Maloney, *Cellulose*, 2021, **28**, 8939–8969.
4 Y. Doi, S. Kitamura and H. Abe, *Macromolecules*, 1995, **28**, 4822–4828.
5 H. Sashiwa, R. Fukuda, T. Okura, S. Sato and A. Nakayama, *Mar. Drugs*, 2018, **16**, 34.
6 S. Wang, K. A. Lydon, E. M. White, J. B. Grubbs, E. K. Lipp, J. Locklin and J. R. Jambeck, *Environ. Sci. Technol.*, 2018, **52**, 5700–5709.
7 C. Kato, A. Honma, S. Sato, T. Okura, R. Fukuda and Y. Nogi, *High Pressure Res.*, 2019, **39**, 248–257.
8 E. Amasawa, T. Yamanishi, J. Nakatani, M. Hirao and S. Sato, *Environ. Sci. Technol.*, 2021, **55**, 3380–3388.
9 T. Kabe, C. Hongo, T. Tanaka, T. Hikima, M. Takata and T. Iwata, *J. Appl. Polym. Sci.*, 2015, **132**, 41258.
10 F. Selli, R. Hufenus, A. Gooneie, U. H. Erdoğan and E. Perret, *Polymers*, 2022, **14**, 200.
11 W.-Y. Huang, S. Suye and S. Fujita, *ACS Appl. Bio Mater.*, 2021, **4**, 7456–7466.
12 W.-Y. Huang, N. Hashimoto, R. Kitai, S. Suye and S. Fujita, *Polymers*, 2021, **13**, 2273.
13 A. M. Díez-Pascual, *Polymers*, 2021, **13**, 2233.
14 D. Li, J. Fu and X. Ma, *Polym. Compos.*, 2020, **41**, 381–390.
15 J. Dong, W. Zhou, Y. Su and X. Ma, *Polym. Compos.*, 2020, **41**, 4538–4549.
16 L.-P. Wu, M. You, D. Wang, G. Peng, Z. Wang and G.-Q. Chen, *Polym. Chem.*, 2013, **4**, 4490.
17 W. Arifin and T. Kuboki, *Polym. Compos.*, 2018, **39**, 491–503.
18 Q.-F. Guan, H.-B. Yang, Z.-M. Han, L.-C. Zhou, Y.-B. Zhu, Z.-C. Ling, H.-B. Jiang, P.-F. Wang, T. Ma, H.-A. Wu and S.-H. Yu, *Sci. Adv.*, 2020, **6**, eaaz1114.
19 A. Iwatake, M. Nogi and H. Yano, *Compos. Sci. Technol.*, 2008, **68**, 2103–2106.
20 K. Benhamou, H. Kaddami, A. Magnin, A. Dufresne and A. Ahmad, *Carbohydr. Polym.*, 2015, **122**, 202–211.
21 K.-Y. Lee, Y. Aitomäki, L. A. Berglund, K. Oksman and A. Bismarck, *Compos. Sci. Technol.*, 2014, **105**, 15–27.
22 M. Yamagata, H. Uematsu, Y. Maeda, S. Suye and S. Fujita, *J. Fiber Sci. Technol.*, 2021, **77**, 223–230.
23 A. Anžlovar, A. Krajnc and E. Žagar, *Cellulose*, 2020, **27**, 5785–5800.
24 A. Anžlovar, I. Švab, A. Krajnc and E. Žagar, *Cellulose*, 2021, **28**, 7813–7827.
25 S. Shrestha, R. A. Chowdhury, M. D. Toomey, D. Betancourt, F. Montes and J. P. Youngblood, *Cellulose*, 2019, **26**, 9631–9643.
26 M. Rincón-Iglesias, E. Lizundia, D. M. Correia, C. M. Costa and S. Lanceros-Méndez, *Cellulose*, 2020, **27**, 3821–3834.
27 J. Wu and G.-H. Ma, *Small*, 2016, **12**, 4633–4648.
28 J. L. Sanchez-Salvador, A. Balea, M. C. Monte, A. Blanco and C. Negro, *Appl. Sci.*, 2019, **9**, 359.
29 F. Cherhal, F. Cousin and I. Capron, *Biomacromolecules*, 2016, **17**, 496–502.
30 X. Liu, X. Qi, Y. Guan, Y. He, S. Li, H. Liu, L. Zhou, C. Wei, C. Yu and Y. Chen, *Carbohydr. Polym.*, 2019, **224**, 115202.
31 Y. He, X. Liu, X. Qi, Y. Guan, S. Li, H. Liu, L. Zhou, C. Wei and C. Yu, *Polym. Adv. Technol.*, 2020, **31**, 2676–2686.

32 Y. Zhang, L. Cui, H. Xu, X. Feng, B. Wang, B. Pukánszky, Z. Mao and X. Sui, *Int. J. Biol. Macromol.*, 2019, **137**, 197–204.
33 Y. Nagakawa, S. Fujita, S. Yunoki, T. Tsuchiya, S. Suye, K. Kinoshita, M. Sasaki and T. Itoi, *J. Mater. Chem. B*, 2022, **10**, 4375–4385.
34 T. Tsuji, K. Tsuboi, S. Yokota, S. Tagawa and T. Kondo, *Biomacromolecules*, 2021, **22**, 620–628.
35 C. Xiong, Z. Quan, H. Zhang, L. Wang, X. Qin, R. Wang and J. Yu, *Appl. Surf. Sci.*, 2020, **532**, 147400.
36 Y. Wakuda, S. Nishimoto, S. Suye and S. Fujita, *Sci. Rep.*, 2018, **8**, 6248.
37 S. Fujita, Y. Wakuda, M. Matsumura and S. Suye, *J. Mater. Chem. B*, 2019, **7**, 6556–6563.
38 R. A. Rebia, N. S. B. Sadon and T. Tanaka, *Nanomaterials*, 2019, **9**, 1665.
39 B. Hammouda and D. L. Ho, *J. Polym. Sci., Part B: Polym. Phys.*, 2007, **45**, 2196–2200.
40 A. K. Maurya, L. Weidenbacher, F. Spano, G. Fortunato, R. M. Rossi, M. Frenz, A. Dommann, A. Neels and A. Sadeghpour, *Nanoscale*, 2019, **11**, 7176–7187.
41 L. Wang, D. J. Gardner and D. W. Bousfield, *Polym. Eng. Sci.*, 2018, **58**, 793–801.
42 W. Leng, J. Li and Z. Cai, *Polymers*, 2017, **9**, 597.
43 L. G. Greca, M. Rafiee, A. Karakoç, J. Lehtonen, B. D. Mattos, B. L. Tardy and O. J. Rojas, *ACS Nano*, 2020, **14**, 12929–12937.
44 P. Hughes, S. Fujita, T. Satomura and S. Suye, *Mater. Lett.*, 2012, **72**, 88–91.
45 R. Arjmandi, A. Hassan, M. K. M. Haafiz and Z. Zakaria, in *Natural Fiber-Reinforced Biodegradable and Bioresorbable Polymer Composites*, Elsevier, 2017, pp. 111–136.
46 F. Li, X. Xu, J. Yu and A. Cao, *Polym. Degrad. Stab.*, 2007, **92**, 1053–1060.
47 I. Taniguchi, S. Nakano, T. Nakamura, A. El-Salmawy, M. Miyamoto and Y. Kimura, *Macromol. Biosci.*, 2002, **2**, 447–455.
48 T. Morohoshi, K. Ogata, T. Okura and S. Sato, *Microbes Environ.*, 2018, **33**, 19–25.
49 C. Volant, E. Balnois, G. Vignaud, A. Magueresse and S. Bruzaud, *J. Polym. Environ.*, 2022, **30**, 2254–2269.
50 W.-Y. Huang, T. Hibino, S. Suye and S. Fujita, *RSC Adv.*, 2021, **11**, 5703–5711.

